Design and results of Differential Microwave Radiometers (DMR) on COBE

Michael A. Janssen
Samuel Gulkis

Jet Propulsion Laboratory, California Institute of Technology
4800 Oak Grove Drive, Pasadena, CA 91109

Charles L. Bennett
Alan J. Kogut

NASA Goddard Space Flight Center, Code 685
Greenbelt, MD 20771

ABSTRACT

The Differential Microwave Radiometer (DMR) experiment on the Cosmic Background Explorer is in the final year of a scheduled four years of operation to measure large- and intermediate-scale anisotropies in the Cosmic Microwave Background (CMB). The DMR instrument comprises two independent radiometers at each of three frequencies, 31.5, 53, and 90 GHz, where the frequencies were chosen to best separate the CMB from the foreground emissions from galactic dust and electrons. The radiometers switch symmetrically between two beams of 7° Half-power width separated by 60° on the sky, and provide a data set of sky brightness temperature differences that allows the determination of all-sky maps of brightness temperature variations at 7° resolution. Data from the first year's operation were used to produce maps of unprecedented sensitivity in which the long-sought intrinsic anisotropies were identified. Three more years of data will ultimately be available to refine the anisotropy measurements.

1. HISTORY

Several anisotropy experiments (three microwave and one far-IR) along with other cosmic background experiments were proposed in response to the 1974 NASA Announcements of Opportunity AO-6 and AO-7 for new Explorer-class space missions[1-3]. A subset of the original proposers was selected by NASA to combine their measurement concepts into a single dedicated mission. They formed the core of the COBE Science Working Group, and worked to define a unified mission to explore the cosmic background. The outcome in 1977 was a proposal to NASA containing the complementary three-experiment approach that became the present COBE mission[4]. The instrument Principal investigators were identified afterward, including George Smoot as the Principal Investigator for the DMR experiment. The goal of the DMR experiment was to obtain definitive measurements of the CMB anisotropies, with the objective of measuring the large-scale CMB brightness variations over the entire sky with an accuracy limited primarily by the ability to account for the foreground emissions.

The original DMR experiment was planned as a four-frequency experiment that included radiometers at 23 GHz but which had the same symmetric differential design and experiment approach as the final version. Two factors affected the final design. First, the launch date as projected early in the project ultimately slipped by many years. Secondly, construction originally began on a spacecraft and complement of instruments that were designed for a shuttle launch into near-polar orbit from the Vandenberg launch site, the plans for which had to be scrapped as a result of the Challenger disaster in 1986. As the launch date slipped the microwave techology in the DMRs became outdated; further, the need for greater sensitivity and a shift in spectral emphasis became apparent as more was learned of the foregrounds from ongoing astronomical research. Consequently, in 1984, decisions were made to eliminate the 23 GHz radiometers, to include newer technology into the remaining instruments, and to incorporate passive cooling into the designs of the critical 53 and 90 GHz radiometers to achieve further

improvement in their sensitivities. The 23 GHz radiometers were replaced by a series of balloon flights with a 19 GHz maser receiver system-5. The elimination of the shuttle polar orbiter forced a major redesign of the spacecraft to enable a Delta launch, one consequence of which was a modification to the 31.5 GHz radiometers so that the new spacecraft would fit the envelope of the Delta shroud. COBE was finally launched on November 18, 1989, and the discovery of CMB anisotropies was announced by the DMR team on April 23, 1992.

2. INSTRUMENT DESIGN

A thorough description of the DMR design has been given by Smoot *et al.*[6], and we summarize here the main features of this design. The DMR instrument comprises a pair of effectively independent radiometers at each of the frequencies: 31.5, 53, and 90 GHz. Simplified schematics of a typical radiometer pair are given in Figure 1. Each radiometer is based on a Dicke-switched heterodyne receiver scheme and produces an output that is proportional to the difference between the antenna temperatures of two identical horn antennas. The axes of these horns subtend an angle of 60°, and are oriented on the spacecraft so that the spacecraft spin axis bisects this angle. On command, noise sources inject broadband noise power into the circuit just following the antenna for calibration. In flight the noise sources are turned on consecutively for approximately one minute each every two hours. The noise sources are weakly coupled into the radiometer circuit to produce a change in antenna temperature of approximately 2 K, well within the ±4 K range of the lock-in amplifiers but of sufficient strength to permit measurement to much better than 0.1 % in one minute. Each noise source is coupled to both radiometers of a frequency pair to provide a calibration cross-check. The local oscillator is common to both receivers of the pair. The horn antennas are independent in each of the 53 and 90 GHz radiometers,

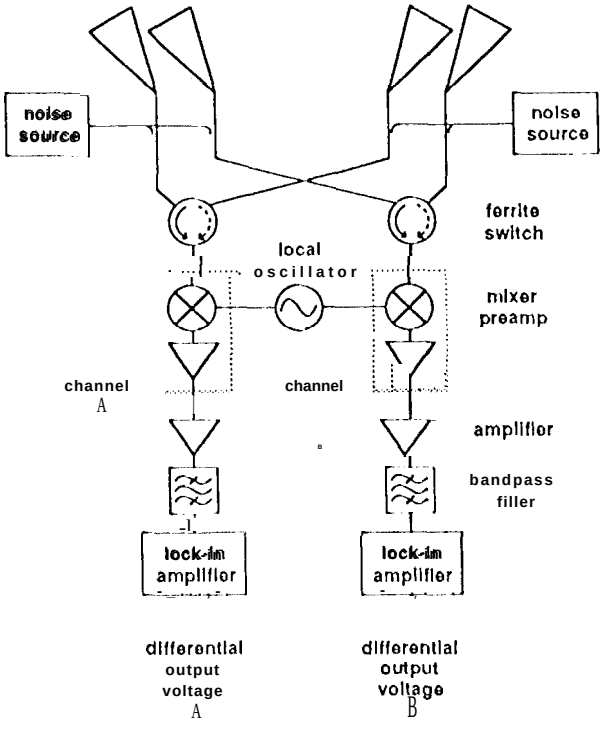

Figure 1: Simplified schematic of DMR 53 or 90 GHz radiometer pair. See Smoot *et al.*[6] for a more complete circuit. The 31.5 GHz schematic is the same except that the antennas in each direction are shared using ortho-mode transducers to receive each circular polarization.

but are shared between the 31.5 GHz radiometers because of size constraints (the 31.5 GHz radiometer schematic is otherwise as shown in Figure 1). This sharing is accomplished by using both circular polarizations received by each horn, separating them into the otherwise independent radiometers through orthomode transducers that follow the horns. The 53 and 90 GHz antennas all receive linear polarizations parallel to the plane of the horn opening angle.

The antennas are wavelength-scaled conical corrugated scalar feedhorns designed specifically for high off-axis signal rejection, and have been used in previous anisotropy experiments. The sidelobe performance was demonstrated on a prototype at 31.4 GHz[7], and measured for the flight horns prior to launch[8].

The switched outputs of each radiometer are sent to individual lock-in amplifiers that convert the intermediate-frequency powers into proportional voltages, then to synchronous demodulators that recover the differential signals from these voltages, and finally to integration circuits that average the differential voltages for contiguous 0.5-sec intervals. The averaged volts.gcs are sampled each 0.5 sec by external data electronics units and incorporated into the spacecraft data stream.

Each pair of radiometers is packaged as a single unit with a mechanical design that allows the thermal loads to be distributed symmetrically with respect to the horn antennas, and a thermal design to allow precise temperature control of those components of the radiometers that are critically temperature-sensitive.. In addition, the horn throat sections are thermally coupled in each radiometer by a massive aluminum thermal short across each horn pair to minimize potential thermal gradients, variations in which might appear as transient signals in the differential output. In the 53 and 90 GHz units all circuit elements from the horn throats through the mixer-preamplifiers are thermally isolated in a critical region enclosure which is radiatively cooled to space and temperature-controlled to maintain an enclosure temperature of 140 K. "The remaining elements including the noise sources, local oscillators, and amplifiers are located in a warm enclosure controlled at a temperature near 290 K. The entire 31.5 GHz unit is maintained at a temperature near '270 K.

Regulated instrument power is provided by two external units, each of which supplies power to one radiometer of each frequency pair. Two additional units digitize the analog signals from the radiometers according to the same connection scheme, and provide communication with the spacecraft.

3. EXPERIMENT DESIGN

The DMR experiment takes advantage of symmetries in instrument design and observational approach to minimize systematic errors and to facilitate their accounting. For example, small asymmetries in the radiometers produce offsets in the differential] outputs which, although nearly constant and small in the context of radiometry ($\leq$ 1 K), are nevertheless large compared to the differential sky signal ($\leq$ few mK). To a good approximation the 75-sec spacecraft rotation period interchanges the beams on the sky every 37.5 see, so that in principle these offsets may be accounted for and the true differential temperature of the sky may be obtained by a double-differencing technique. In the actual ground processing the offsets are allowed to be functions of time that vary slowly compared to the spacecraft rotation period ant! are solved for and removed from the time series of differential measurements, giving an effectively equivalent subtraction. Also, data are rejected when the Earth is 1" below the Earth-Sun shield or higher (5% of data), when the Moon is within 25° of an antenna boresight (6.6 % of data), when the spacecraft telemetry or attitude solution is of poor quality (1 .5% of data), or when any datum deviates from the daily mean by more than 5 standard deviations (<.001 % of data).

With the offset subtraction and the application of a calibration factor to convert the remaining data from raw telemetry units to antenna temperature, the data set from each radiometer consists of a set of brightness temperature differences of points on the sky separated by the horn opening angle of 60". The one-year precession period of the near-polar COBE orbit ensures that all such differences on the sky

are obtained after six months of continuous observation. It was recognized early on that such a data set could be used to obtain a relative map of sky brightness by a linear least-squares fitting procedure[9]. For example, consider a tesselation of the sky into a sufficiently large number N of approximately uniform pixels so that the vector **t** with elements $T_i, 1 \leq i \leq N$, represents a map of the sky at a resolution comparable to the DMR resolution of 7°. We represent the data set as the matrix S_{ij}, whose elements are the average of all measurements between the i^{th} and j^{th} pixels for those pairs that are pierced by directions separated by 60°, and zero otherwise. For the purpose of illustration, let us take the simple case in which each such measurement has the same uncertainty σ. Then a chi-squared sum may be written as

$$\chi^2 = \frac{1}{2} \sum_{i=1}^{N} \sum_{(j)_i}^{M_i} \left[\frac{(T_i - T_j S_{ij})}{\sigma} \right]^2 \qquad 1.$$

where the notation $(j)_i$ indicates the set of M_i pixels connected to the i^{th} pixel by a differential measurement and the factor of 1/2 ensures that each measurement is counted once. The map may be determined as the vector **t** that minimizes χ^2. Differentiating χ^2 with respect to the T_i and setting the result to zero yields the normal equations

$$T_i - \frac{1}{M_i} \sum_{(j)_i}^{M_i} T_j = \frac{1}{M_i} \sum_{(j)_i}^{M_i} S_{ij} \qquad 2.$$

which comprise a set of N linear equations to be solved for the map elements T_i. Thus the determination of a sky map from differential measurements is an exercise in linear algebra.

These equations may be expressed in matrix form

$$\mathbf{M} \bullet \mathbf{t} = \mathbf{D} \qquad 3.$$

where $M_{ii}=1, M_{ij(j\neq i)}=1/M_i$ if j is contained in $(k)_i$ or zero otherwise, **t** is the map vector, and the elements of the measurement vector **D** are the sums on the right-hand side of Eq. 2. M is readily shown to be singular, which is to be expected inasmuch as the differential measurements are insensitive to the absolute, temperature level of the map. This singularity is easily removed by arbitrarily specifying one map temperature. M is also large (N = 1000 for 7° resolution, while N = 6144 is used in the DMR processing), and sparse, since the vast majority of elements M_{ij} are zero, so that iterative sparse matrix techniques are used to invert Eq. 3.

Subsequently this approach has been expanded into a more sophisticated sparse-matrix inversion which uses the entire set of time-series differential measurements instead of the averaged pixel difference data, and solves for the amplitudes of assumed time-varying error functions as well as the map vector[10,11]. In this approach the normal equations become

$$\mathbf{M} \bullet \mathbf{t} = \mathbf{V}^t \bullet \mathbf{d} \qquad 4.$$

where

$$\mathbf{M} = \mathbf{V}^t \bullet \mathbf{V} \qquad 5.$$

and **V** is a rectangular matrix of small dimension N + n, where n represents the number of functions whose amplitudes are sought, and long dimension N_{obs}, which is the number of 0.5-sec integrations in the time series data. Each row of V (i.e., across the N + n dimension) contains 1 for the pixel pierced by

the positive horn, -1 for the pixel pierced by the negative horn and zero for the remainder of the map pixel elements, and the evaluated function values for the function elements from N + I to N + n. The N-t n-dimensional map vector **t** now includes the error function amplitudes E_q, $1 \le q \le II$ in addition to the pixel temperatures, anti the N_{obs}-dimensional data vector **d** is the time series of differential measurements.

This reformulation permits one to search for and remove anticipated systematic errors that depend predictably on known parameters of the observation. An important example of such an error is the susceptibility of the differential output to the strength and alignment of the Earth's magnetic field caused by otherwise hard-to-measure magnetic susceptibilities of radiometer components (the ferrite Dicke switches, for example). "l'his type of susceptibility produces a signal in the differential output which is similar to a signal from sky brightness variations, but which can be identified in the long-term time series by its unique correlations with the radiometer orientation in the magnetic field. Other systematic errors which have been searched for in the time series data include emission from the Earth diffracted around the COBE Sun-Earth shield, RFI from geosynchronous satellites, and instrumental thermal susceptibilities. These errors are not easily handled by the above formalism because of either the lack of a known functional form for the error or sufficiently sensitive knowledge of key parameters, but have been searched for by mapping as above in coordinate frames in which the suspect signals arc likely to be coherent (e.g., Earth- or spacecraft body-centered frames). Limits for these and other forms of systematic errors are discussed by Kogut *et al.*[12].

4. CALIBRATION

The DMR radiometers were absolutely calibrated prior to launch using temperature-controlleci warm anti cold loads in a thermal-vacuum test chamber. These calibrations were transferred to space via the *noise* sources under the assumption that the latter remained stable from the time of the chamber measurements through launch. Additional methods for independent absolute calibration use observations of the Moon anti the modulation of the CMB dipole as the Earth goes around the Sun. Relative calibration is also provided by the noise sources and by the Moon and dipole observations, and is necessary to ensure that instrument gain variations do not generate artifacts in the maps.

4.1 Absolute calibration

The ground-based calibrations have been described by Bennett *et al.*[13], and arc estimated to yield absolute accuracies ranging from 1 % to 3% depending on radiometer. These calibrations have formed the basis for the anisotropy results presented to date. 'l'he data obtained in flight offer additional methods for independent absolute calibration, also described by Bennett *et al.*,[13] which are valuable for the crosschecking and possible improvement of these calibrations.

The Moon passes through the plane of the COBE orbit twice per lunar orbit (see Figure 2), where it is seen frequently by the DMRs. The microwave, brightness temperature of the Moon can be predicted as a function of frequency anti lunar phase to the extent that the thermophysical properties of the upper few centimeters of is surface are known, Using an emission mode] based on Apollo *in situ* data, Keihm[14] has developed a uniform "average" global model for spatially unresolved lunar microwave flux measurements for use in calibrating the COBE DMRs. The 0.5° angular diameter of the Moon is much smaller that a DMR beamwidth, so that the disk-averaged brightness temperature along with its solid angle and emission centroid are sufficient for this purpose. Figure 2 shows the disk- averaged brightness temperatures predicted by this model at the DMR frequencies. As described by Bennett *et al.*[15], the Moon observations by the DMRs are analyzed in a least-squares fitting procedure to determine mean pointing offsets and the on-axis antenna temperatures. These temperatures are. used with the model predictions and knowledge of the DMR beam solid angles from ground-based data to determine the DMR gains. Accounting for uncertainties in the model, Keihm estimated an overall accuracy in average

disk temperature of about 4% near ±90° phase, and an additional 2% with phase within the DMR observational range.

The velocity of the spacecraft with respect to the CMB varies significantly during the year as the Earth goes around the Sun, which produces significant variations in the CMB dipole anisotropy through the Doppler effect. For example, the COBE orbit around the Earth and the Earth's velocity around the Sun produce modulations of about 0.07 mK and 0.3 mK, respectively, of the ~3 mK dipole amplitude. The velocity variations are well known, so the assumption that the CMB spectrum is Planckian (now well validated by the FIRAS experiment [15]) leads to extremely accurate predictions for these modulations[13, 16]. Analysis of the first year's data has led to absolute calibrations using this technique with uncertainties that are limited by the noise of the radiometers and range from 2.8% for the 53A radiometer to 6.8% for the 31A radiometer. These should improve by a factor of two after four years.

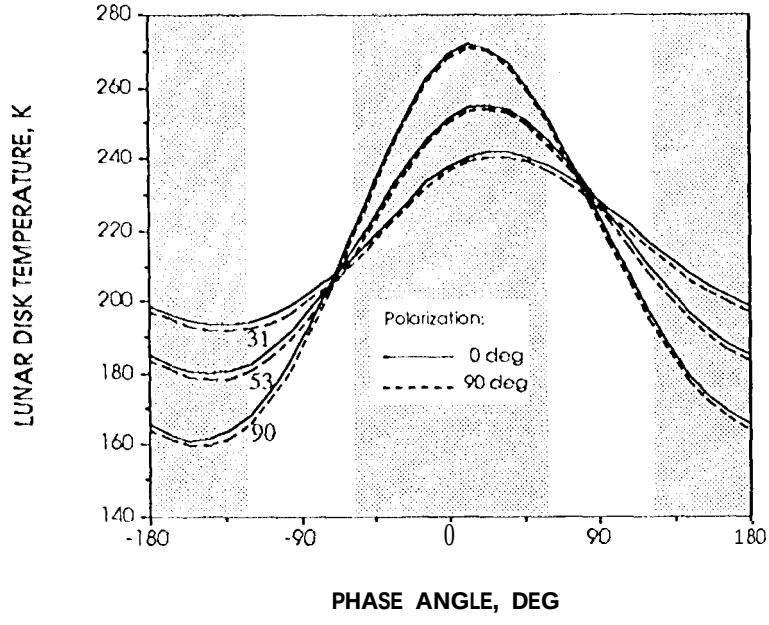

Figure 2: Keihm's model for the disk-averaged lunar brightness temperature as a function of phase and polarization at the DMR frequencies. The DMRs view the Moon only in the unshaded regions.

A further calibration approach which remains to be explored is the use of the. dipole amplitude itself. The precision of the DMR dipole amplitude measurement after one year ranges from 0.5% in the 53A radiometer to 1.3% in the 31B radiometer[16], while the dipole amplitude has been formally determined from the FIRAS data to an accuracy of 0.5% (95% CL) by Fixsen *et al.*[17]. The DMR precision quoted above includes instrument noise and systematics (e.g., residual magnetic susceptibility), but not galactic contamination, which increases these errors to 0.8% and 1.9% respectively. Provided that residual Galactic contamination in both the FIRAS and DMR can be accounted for and that possible deviations from a Planck spectrum are considered, the dipole amplitude can be used to transfer the precise FIRAS absolute calibration to the DMR with a potential improvement at all DMR frequencies.

4.2 Relative calibration

The gain of each radiometer may vary during the course of the mission. If the noise sources remain stable, then these gain variations can be monitored and removed using the noise source outputs. If the noise sources themselves vary, however, then additional references must be used. Both noise sources are seen in each radiometer of a pair, so that the events of an individual noise source output fluctuation or a radiometer gain change can be readily identified. The general case of both gain and noise source variations requires an external source for identification, however.

Both the Moon and the CMB dipole provide standard candles to track calibration drifts on time scales of several weeks or longer. When it is within the DMR scan path, the Moon provides a source that can be measured by each radiometer to better than 1 % in total flux each orbital pass. A drawback is that the strong phase dependence of this flux cannot be completely removed by an *a priori* model, and the same is true to a lesser extent for annual effects due to the varying Earth-Sun distance. Lunar observations previously presented through the first ~500 days have shown a two-week interleaved 5% phase-dependent systematic error (~4% variation from first to third quarters and ~2% variation within 300 of each quarter), and a sinusoidal annual variation of about 2%. [13]

The differences between the observed lunar signal and the predicted lunar model can be expected to be repeatable in both phase and Earth-Sun distance. We have added empirical functions (quadratic phase anti sinusoidal annual terms) to the Kheim lunar model to remove these variations from the observed lunar calibration, in effect forcing the Moon to act as a standard candle referenced to a single (arbitrary) phase and time of year. Figure 3 shows the changes, in percent, of the ratio of the resulting lunar standard to the calibration derived from the on-board noise sources, for both channels of the 53 and 90 GHz radiometers. Each point represents approximately one day of lunar observations compared to the average of all noise source calibrations during this period.

Ratioing the lunar gains with the gains from the noise diodes removes the effects of radiometer gain variations, but does not remove variations in the mean output of the two noise sources (the noise source gain is based on the sum of the outputs from the two noise source firings seen in each radiometer). Insofar as the fitting has removed residual Moon model imperfections, the residuals in Figure 3 show variations in the mean noise source outputs, The solid lines show linear fits to the residuals and indicate slow decreases of less than 0.1 % per year in the mean 53 GHz noise source outputs, and approximately $_{0.8\%}$ per year in the mean 90 GHz noise source outputs. The scatter is in the range 0.3% - 0.4% for the four radiometers and is consistent with the uncertainty in the determination of the Moon signal amplitude represented by each point, which is the dominant source of uncertainty. This analysis is preliminary and the individual noise sources have not yet been cross-compared over the entire time period shown in Figure 3 to narrow the source of the drifts. Also, the data beyond the first year have not been fully validated.

Kogut *et al.*[12] have examined the effects of potential long-term drifts of the calibration on the sky maps, for example finding a 0.4% per year calibration drift to result in a pixel-to-pixel standard deviation <0.7 μK (95% C.L.). Hence the drifts discussed above have negligible impact cm the measurement of the ~30 μK CMB structure (see below).

5. RESULTS

The calibrated, sorted, and corrected DMR maps are dominated by two principal features, a dipole anisotropy and the emission from the Galactic plane, both of which are readily visible in the maps. The dipole anisotropy is present in all of the channels with an average thermodynamic temperature amplitude of 3.365 ± 0.027 mK in the direction l = 264.4° ± 0.3°, b = 48.4°3.0.5° where l and b are galactic longitude and latitude respectively[16]. The dipole amplitude is approximately 0.1% of the background temperature (2.726 K) measured by the COBE-FIRAS experiment. It is difficult to

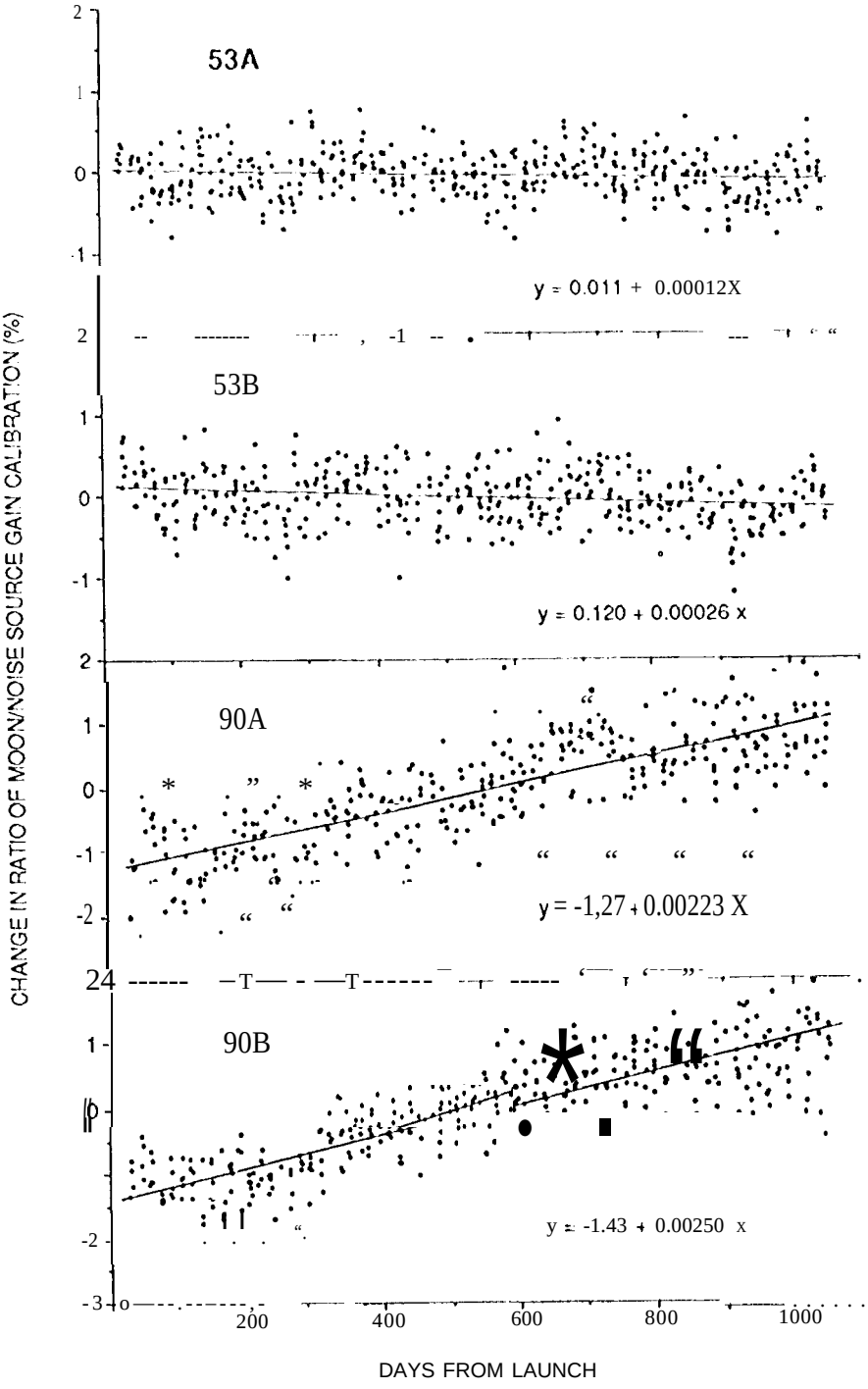

Figure3: Percentage deviation of Moon/noise source gain ratio from unity after removal of empirically-determined systematic error functions of lunar phase and year from the nominal Moon model. "l'he analysis is based on preliminary data after the first year, but indicates slow decreases of approximately 0,170 anti 0.8% per year in the sum of noise source outputs in the 53 and 90 GHz radiometers respectively.

interpret the cosmological significance of the dipole - it could result from motion of the Solar system with repect to the CMB, or it could be intrinsic to the CMB itself. The large (120: 1) ratio of dipole to quadrupole amplitude and the agreement between the velocities inferred from the CMB dipole and optical, infrared, or redshift surveys are evidence for a Doppler origin of the observed dipole anisotropy. We therefore assume that the entire dipole results from our peculiar velocity with respect to the rest frame of the CMB, and correct the maps for the resulting Doppler effect including the quadrupole caused by second-order terms. The mean, dipole, and kinematic quadruple (MDKQ) are removed from the maps in order to examine the data for higher-orcler anisotropy.

The MDKQ-removed maps show no obvious features away from the Galactic plane. The distribution of the temperatures in the individual 2.6 degree pixels is within a few percent of the expected instrument noise ($\approx$ 150 pK) for the integration times of the measurements. Detection of additional features in the MI~KQ-removed maps requires careful statistical analysis and/or averaging over larger angles. Three methods of analysis which have been used (o search for features are 1) to examine the smoothed map variance, 2) to measure the quadruple and higher order spherical moments of the maps, and 3) to analyze the structure of the correlation function. The application of these statistical techniques has been necessary to arrive at the most significant results from the DMR experiment.

The discovery and interpretation of structure in the DMR maps was reported in a series of papers published in 1992[12,18-20]. Smoot *et al.*[18] have shown the 31,53, and 90 GHz maps as smoothed with a Gaussian of 7° FWHM. Taking into account the intrinsic smoothing by the COBE antenna pattern, this additional smoothing results in a net 10 degree smoothing on the sky. The smoothed maps reveal intrinsic fluctuations in sky temperature as may be deduced from the following basic analysis. The variance of the maps is the quadrature sum of the instrument noise (σ_{DMR}) and the intrinsic fluctuations on the sky (σ_{Sky}):

$$\sigma^2_{Obs} = \sigma^2_{DMR} + \sigma^2_{Sky} \qquad 6.$$

The (A+B)/2 sum maps provide an estimate of σ^2_{Obs} and the (A-B)/2 difference maps provide an estimate of σ^2_{DMR}. Using only the data for $|b| > 20$ degrees, we obtain

$$\sigma_{Sky} = 30 \pm 5\ \mu K \qquad 7.$$

This amplitude is approximately 11 parts per million of the total brightness temperature of the sky. Correlation analysis performed on the *maps* reveals the fluctuations to be consistent with structure all scales observed by the DMR, while spherical analysis gives positive detections of the quadruple and higher moments as well as the dipole.

The primary DMR result related to cosmology is the detection of intrinsic temperature fluctuations on the sky σ_{Sky}. long sought after based on theoretical considerations, these temperature fluctuations are believed to be a manifestation of primeval density perturbations which, in turn, are responsible for the large scale structure of the universe. The DMR maps are consistent with a scale-invariant spectrum of such perturbations. Structures as large as hundreds of millions of light years have previously been measured with ground based telescopes, The structures measured by DMR are even larger, stretching across the whole sky. They are the largest structures ever observed.

Large scale density fluctuations in the early universe are believed to have provided the gravity fields that shaped the hierarchical spatial structures seen today, including clusters and superclusters of galaxies. The observed temperature fluctuations arise from differential gravitational redshifts of the photons as the photons exit regions with different gravitational potentials in the early universe. This phenomenon is called the Sachs-Wolfe effect. The less bright regions are thus interpreted as originating from regions of higher density. The photons measured with the DMR instrument reflect on the

conditions about 300,000 years after the Big Bang, when the photons were last scattered by free electrons.

Acknowledgements: The COBE DMR represents the efforts of many individuals over the years, including the DMR Principle Investigator George Smoot along with the other members of the COBE Science Working Group, and the many professionals associated with the COBE project at the Goddard Space Flight Center where the. DMR was designed and built, Thanks arc duc to C. Backus, now at JPL, G. Hinshaw of GSFC, and P. Jackson of Hughes STX Corp. for their assistance in assembling the lunar calibration data presented here. COBE is supported by the Astrophysics Division of NASA's Office of Space Science and Applications. Portions of this work were done at the Jet Propulsion Laboratory, California Institute of Technology, under contract with NASA.

6. REFERENCES

1. Mather, J., Thaddeus, P., Weiss, R., Muehlner, D., Wilkinson, D. T., Hauser, M. G., and Silverberg, R. F., "Cosmological Background Radiation Satellite," NASA/Goddard Proposal (1974).

2. Alvarez, L. W., Buffington, A., Gorenstein, M. V., Mast, T. S., Muller, R. A., Orth, C. D., Smoot, G. S., Thornton, D. D., and Welch, W. J., "Observational Cosmology: The Isotropy of the Primordial Black Body Radiation," UCBSSL 556/75 Proposal to NASA (1974).

3. Gulkis, S., Carpenter, R. L., Estabrook, F. B., Janssen, M. A., Johnston, E. J., Reid, M. S., Stelzried, C. T., anti Wahlquist, H. D., Cosmic Microwave Background Radiation Proposal, NASA/JPL Proposal (1974).

4. Boggess, N. W., *et al.*, "*The* COBE Mission: Its Design and Performance Two Years after launch," *Ap.J.* 396,420-429 (1 992).

5. Boughn, S, P., Cheng, E. S., Nottingham, D. A., and Fixsen, D. J., *Rev. Sci. Instr.* 61, 158 (1990).

6. Smoot, G. F., *et al.*, "*COBE* Differential Microwave Radiometers: instrument Design and Implementation," *Ap. J.*, 360,685-695 (1990).

7. Janssen, M. A., Bednarczyk, S. M., Gulkis, S., Marlin, H. W. and Smoot, G. F., "Pattern Measurements of a Low-Sidelobe Horn Antenna," *IEEE Trans. Ant. Prop.*, **AP-28**, 759-763 (1979).

8. Toral, M. A., Ratliff, R. B., Lecha, M, C., Maruschak, J. G., Bennett, C. I,., and Smoot, G. F., "Measurements of Very Low-Sidelobe Conical Horn Antennas," *IEEE Trans. Ant. Prop.*, **AP-37**, 171-176(1989).

9. Gulkis, S., Janssen, M. A., and Olsen, E. T., "A Method of obtaining Temperature Maps from the COBE Differential Data," COBE memorandum of January 30, 1978.

10. Torres *et al.*, in "Data Analysis in Astronomy 111," V. di Gesu, L. Scarsi and M, C. Maccarone, eds., Plenum, New York, 319 (1989).

11. Janssen, M. A, and Gulkis, S., "Mapping the Sky with the COBE Differential Microwave Radiometers", in The Infrared and Submillimeter Sky after COBE, Eds. M. Signore and C. Dupraz, Kluwer Academic Publishers, 391-408 (1992).

12. Kogut, A., *et al.*, "COBE Differential Microwave Radiometers (DMR): Preliminary Systematic Error Analysis", *Ap.J.* **401**, 1-18 (1992).

13. Bennett, C. 1.., *et al.*, "COBE Differential Microwave Radiometers (DMR): Calibration Techniques", *Ap.J. 391,466-482* (1992).

14. Keihm, S. J., JPL Internal Memo, May 2, 1983.

15. Mather, J. C., et *al.*, "Measurement of the Cosmic Microwave Background Spectrum by the COBE FIRAS", submitted to *Ap.J. (1993).*

16. Kogut, A., *et al.*, "Dipole Anisotropy in the *COBE*-DMR First-Year Sky Maps, " submitted to *Ap.J.* ***(1993).***

17. Fixsen, D. J., *et al.*, "Cosmic Microwave Background Dipole Spectrum Measured by the COBE FIRAS," submitted to *ApJ. (1993).*

18. Smoot, G.F., *et al.*, "Structure in the COBE Differential Microwave Radiometer First-Year Maps", *Ap.J. 396,1 .1-1.5* (1992).

19. Wright, E. I.., et al., "Interpretation of the Cosmic Microwave Background Anisotropy Detected by the COBE Differential Microwave Radiometer", *ApJ. 396,1.13-1.18* (1992).

20. Bennett, C. L., *et al.*, "Preliminary Separation of Galactic and Cosmic Microwave Emission for the COBE-DMR", *Ap.J.* **396**:L7-L12 (1992).